Free-Energy Landscape of the Helical Wrapping of a Carbon Nanotube by a Polysaccharide

ARTICLE *in* THE JOURNAL OF PHYSICAL CHEMISTRY C · JANUARY 2011

Impact Factor: 4.77 · DOI: 10.1021/jp111981y

4 AUTHORS:

Yingzhe Liu
Xi'An Modern Chemistry Research Institute
17 PUBLICATIONS **88** CITATIONS
SEE PROFILE

Chris Chipot
French National Centre for Scientific Researc…
163 PUBLICATIONS **11,818** CITATIONS
SEE PROFILE

Xueguang Shao
Nankai University
230 PUBLICATIONS **3,575** CITATIONS
SEE PROFILE

Wensheng Cai
Nankai University
201 PUBLICATIONS **2,606** CITATIONS
SEE PROFILE

THE JOURNAL OF PHYSICAL CHEMISTRY C

ARTICLE

pubs.acs.org/JPCC

Free-Energy Landscape of the Helical Wrapping of a Carbon Nanotube by a Polysaccharide

Yingzhe Liu,[†] Christophe Chipot,[‡,§] Xueguang Shao,[†] and Wensheng Cai*[,†]

[†]College of Chemistry, Nankai University, Tianjin 300071, People's Republic of China

[‡]Theoretical and Computational Biophysics Group, Beckman Institute, University of Illinois at Urbana−Champaign, Urbana, Illinois 61801, United States

Supporting Information

ABSTRACT: Carbon nanotubes wrapped by polysaccharide chains like chitosan (CHTS) or its derivatives through noncovalent decoration have been shown to condense effectively and deliver DNA for gene therapy. Despite the importance of these novel nanoscale materials, the detail of the microscopic structure and underlying interaction mechanism is still fragmentary. In the present work, the complex formed by CHTS and a single-walled carbon nanotube (SWNT) has been investigated by means of atomistic molecular dynamics (MD) simulations to explore its propensity toward self-assembly, together with its structural properties in an aqueous environment. The present results reveal that CHTS can wrap spontaneously the tubular surface by regulating backbone torsional stress upon van der Waals attraction by the SWNT, resulting in a steady, right-handed helical conformation. The free-energy landscape characterizing the wrapping process of the CHTS chain from a straight conformation to a tight helical one brings to light two energetically favored helical conformations corresponding to distinct pitches. In addition, the degree of deacetylation of the polysaccharide chain, but not the pH, induces pronounced fluctuations in the geometrical properties of the helix.

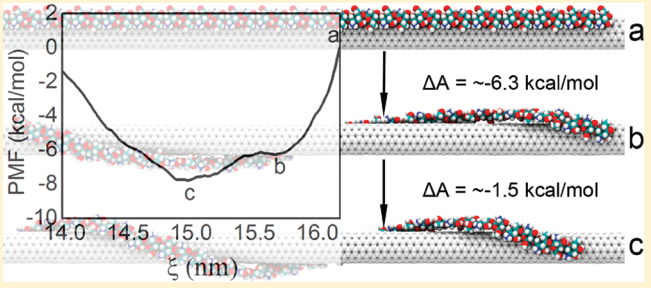

1. INTRODUCTION

Gene therapy has been the object of broad attention as a potential treatment for various genetic disorders through the introduction of native, intact genes into cells to replace or alter defective or anomalous ones.[1] To be successful, this approach requires that the therapeutic DNA be effectively condensed into tight bundles and then trafficked toward its target location. Suitable cationic molecules such as polyamines, lipids, and dendrimers have been widely employed in packaging DNA into nanoparticles,[2−4] which proceeds mainly by virtue of noncovalent interactions with the electronegative grooves of DNA. Research efforts are, therefore, currently focused on designing effective carrier vectors for transporting oligonucleotides.

Carbon nanotubes (CTNs) have been regarded as promising candidates for gene delivery on account of their efficient penetration into living cells,[5] as well as other remarkable properties ranging from high thermal and electrical conductivity, great mechanical strength, to excellent chemical stability.[6] Functionalization of CNTs has been applied to overcome their poor aqueous solubility, paving the way to a variety of potential applications, especially in biomedical research areas as molecular transporters. Dai and coworkers[7−9] put forth that protein and RNA could be trafficked into mammalian cells by means of modified nanotubes. In addition, Bianco and co-workers[10] reported that peptide functionalized CNTs are able to penetrate the plasma membrane and translocate into the cell nucleus. Shortly afterward, they designed a cationic nanotube functionalized by ammonium, which can induce DNA condensation on the tubular surface.[11] De novo design of nanotube-based gene delivery vehicles admittedly represents an effervescent research area of topical interest.

In addition to experimental studies, theoretical investigations, particularly classic molecular dynamics (MD) simulations, have been endeavored to detail the interaction mechanism between DNA and CNT at the atomic level. Klein and co-workers[12−14] analyzed the structure, self-assembly mechanisms, and the energetic properties of these nanoscale complexes in a systematic fashion. They found that a single-strand DNA can adopt a helical conformation by wrapping around the surface of nanotube as a result of the balance of electrostatic and torsional interactions within the sugar−phosphate.[12] The helical structure, however, is merely a local minimum obtained from the free-energy landscape of the DNA−CNT system.[13] Moreover, the nature interactions were further investigated by the calculation of binding free energy between base and CNT.[14] These series studies provide a new

Received: December 16, 2010
Published: January 10, 2011

insight into the understanding of self-assembly of a DNA−CNT hybrid.

A major limitation in the use of CNTs for gene delivery, however, lies in the biocompatibility and cellular toxicity of such compounds. This biological issue, which embraces inflammatory responses, oncogenic effects, and immune defense, must be addressed before therapy for humans can be considered. Chitosan (CHTS) is a naturally occurring polysaccharide with a highly cationic density and a universally accepted nontoxic chemical species due to its remarkable biocompatibility and biodegradability.[15] Experiment showed that decoration of CNTs with CHTS dramatically improves the delivery characteristics of DNA and peptides, while decreasing toxicity of CNTs.[16] Recently, Liu and coworkers[17] demonstrated that CHTS wrapping CNTs yields an appreciably more effective DNA condensation than CHTS itself. This result stems from the fact that CHTS aggregates can be dispersed by CNTs, hence becoming more suitable to interact with DNA. Furthermore, the noncovalent wrapping mode renders CNTs soluble due to preventing the hydrophobic CNTs from aggregating into bundles, while preserving the unique electrical characteristics of these tubular compounds. Such a supramolecular architecture, thus, provides a remarkable potential route for the effective control of gene delivery and expression.

This novel nanomaterial can be utilized not only in gene transfer, but also in a variety of other biotechnological applications ranging from electrochemical biosensor to cellular proliferation matrices.[18,19] Despite the importance of CHTS:CNT complexes, detail of their microscopic structures, their physical properties, and the intermolecular interactions at play is still missing in large measure. Exploring at the atomic level the nature of the interplay of CHTS and CNT species is, therefore, envisioned to complement nicely the available experiments, while helping interpret them.

In the present work, classical, all-atom MD simulations have been performed to investigate the mechanism that underlies the self-assembly in aqueous solution of CHTS and single-walled carbon nanotubes (SWNTs) into heterodimeric complexes. The free energy that delineates the helical arrangement of CHTS around the SWNT was determined using an adaptive biasing force.[20−23] Furthermore, the influence of the pH and the degree of deacetylation on the structural properties of the supramolecular assembly, in particular the helicity of the CHTS chain, was examined.

2. METHODS

2.1. Molecular Models. CHTS consists of randomly distributed *N*-acetyl-D-glucosamine and β-(1,4)-linked D-glucosamine, which is produced by deacetylation of chitin (CHIT, Scheme 1). In the present contribution, only the two typical structural motifs characterized by $x = 0$ and $x = 1$ were considered. The initial coordinates of CHIT and CHTS were taken from available crystal structures.[24,25] On the basis of the unit-cell parameters, 40-mer polysaccharide chains were constructed. Moreover, undecorated and ideal SWNTs were modeled. The atoms of the SWNT were described as sp^2 aromatic carbon parameters of the CHARMM27 force field[26] devoid of a net atomic charge. The equilibrium length of the C−C bonds was 1.42 Å. The position of all SWNT atoms was restrained by means of a weak harmonic potential. To eliminate possible edge effects, an infinite long SWNT was built by sharing the chemical bond between the terminal carbon atoms employing periodic boundary conditions (PBCs). Water molecules in the interior of SWNT were all removed. The general description of the molecular assemblies considered in this study is summarized in Table S1.

Scheme 1. Chemical Structure of Chitin and Chitosan

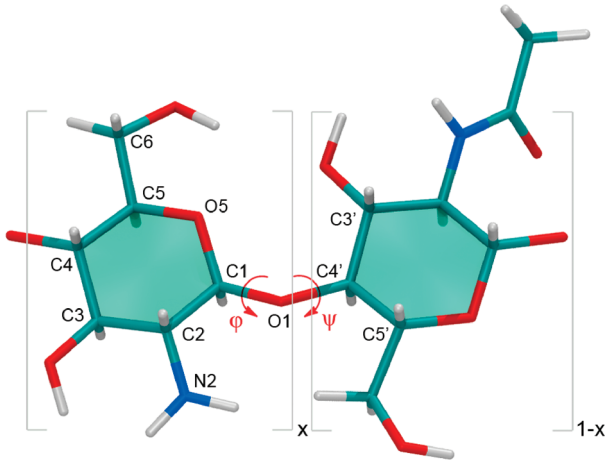

2.2. Molecular Dynamics Simulations. All the atomistic MD simulations described herein were performed using the parallel, scalable MD program NAMD.[27] The specific CSFF[28] parameters for carbohydrate solution simulations and the TIP3P[29] water model were employed to describe the molecular assembly. PBCs were applied in three directions of Cartesian space. The equations of motion were integrated with a time step of 2 fs. Covalent bonds involving hydrogen atoms were constrained to their equilibrium length by means of the SHAKE/RATTLE algorithms.[30,31] Long-range electrostatic forces were evaluated using the particle mesh Ewald (PME) scheme,[32] and a smoothed 12 Å spherical cutoff was applied to truncate van der Waals interactions. Each system underwent 2000 steps of energy minimization to remove poor atomic contacts, 2 ps of heating from 0 to 300 K at fixed volume by reassigning velocities, followed by 500 ps of equilibration at 300 K and 1 atm, respectively, employing Langevin dynamics and the Langevin piston pressure control.[33] Last, production simulations were performed in the NVT ensemble at the same temperature. Visualization and analysis of MD trajectories were carried out with the VMD package.[34]

2.3. Free-Energy Calculations. The free-energy profile along an appropriate order parameter, ξ, describing the conformational transition of a helical polysaccharide chain adsorbed onto the SWNT surface was determined employing the ABF method.[20−23] The order parameter used here was chosen as the distance separating the centroid of the pyranose ring in the 5th and 36th residues, respectively, which is anticipated to eliminate any edge effect. The initial structure for ABF calculations was obtained from the thermalization MD simulations. The reaction pathway, spanning $13.98 \leq \xi \leq 16.18$ nm, was divided into 11 consecutive windows, 0.2 nm wide, wherein was over 10 ns of sampling. Instantaneous values of the force were accrued in bins, 0.01 nm wide. To avoid possible nonequilibrium artifacts, 5000 samples were accumulated in each bin prior to application of the adaptive bias. To improve sampling uniformity, continuity of the average force across neighboring windows, and convergence of the free energy, the overall simulation time was extended incrementally up to 160 ns.

3. RESULTS AND DISCUSSION

3.1. Spontaneous Wrapping in Water. To obtain a microscopic picture of the CHTS−SWNT supramolecular complex and illuminate the interactions underlying self-assembly, an MD

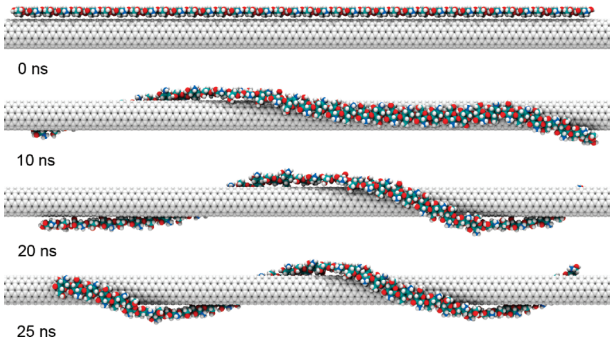

Figure 1. Milestones of the wrapping process obtained from an MD simulation over a 25 ns period. Water molecules and counterions are omitted for clarity.

simulation was carried out, in which the 40-mer polysaccharide chain was separated from the surface of a (6,6) SWNT by about 4 Å. Figure 1 shows milestone configurations in the process of spontaneous assembly extracted from the MD trajectory. Initially, the CHTS segment was organized in a straight conformation, aligned parallel to the SWNT. Driven by van der Waals attraction, the two ends of the CHTS chain began to bend toward the tubular surface. After 10 ns, the CHTS segment curled into a partial helical pattern at one end, while the middle of the polymer conserved its straight conformation. Subsequently, the chain gradually relaxed to wrap the SWNT and form a full helical conformation after ca. 20 ns. The complex of CHTS−SWNT reached past 25 ns an equilibrium structure consisting of a perfect right-handed helix. This loose wrapping structure is in accordance with the available transmission electron microscopy graph.[17,19] This mode is different from the compact wrapping mode of amylose, another kind of polysaccharide, governed by hydrogen bonds between neighboring turns.[35,36] The loose helical conformation gives rise to less need of CHTS for dispersion of CNTs.

To accrue additional statistical data and ascertain that the complex has fully relaxed, the time scale of the simulation was prolonged to 100 ns. The resulting trajectory reveals that the helical conformation is preserved. The pitch of the helix, however, fluctuates on account of the unhampered diffusion of the ends of the CHTS segment along the SWNT. The helical pitch is a crucial parameter used to characterize the overall fold of polymer chains. Here, the pitch was measured on the basis of a fitting procedure.[37] The angle formed by the projected vectors borne by two residues and the corresponding distance between their centroids along the longitudinal axis of the SWNT (see the inset of Figure 2d) were fitted linearly to compute the helical pitch. The slope of the regression line corresponds to the average distance per degree. When the angle is equal to 360°, the measured distance is the pitch of the helix. The angle−distance correlation in the fitting procedure represents the degree of helicity of the structure; that is, if the correlation tends toward 1, the helical conformation is regular and ordered. Only the central 32 monomers of the CHTS chain were selected to calculate the pitch.

Figure 2d shows the time evolution of the pitch of CHTS. Initially, the pitch tends to infinity on account of the straight conformation. As CHTS progressively wraps the SWNT, the pitch decreases and the helical structure becomes increasingly regular. After ca. 22 ns, the pitch reaches a minimum value and then fluctuates steadily. After ca. 70 ns, the helicity deteriorates abruptly as one end of CHTS desorbs from the tubular surface. Ten

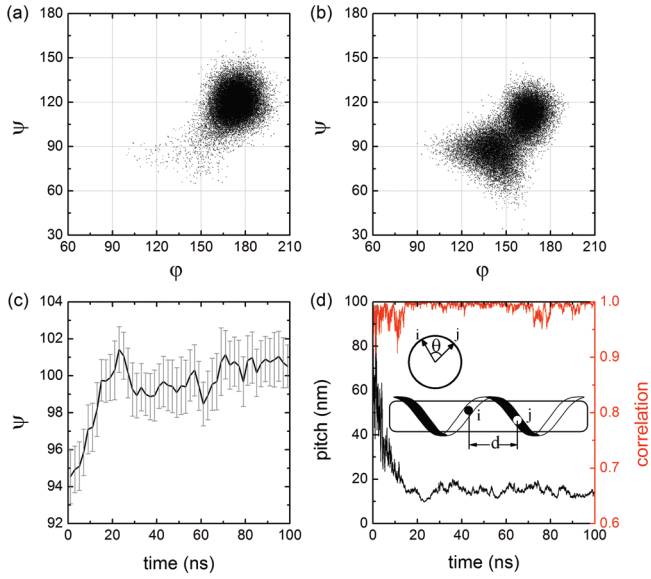

Figure 2. (a) Distribution of the (φ,ψ) backbone torsional without the SWNT and (b) with the SWNT. (c) Time evolution of the average torsional angle ψ. (d) Fluctuations of the pitch (black) and angle−distance correlation (red) as a function of the simulation time. The centroids of the residues of the CHTS chain were used for computing the helical pitch. Two parameters, angle θ and distance d, defined in the inset, were measured, and d was correlated linearly with θ. Inset: Angle θ formed between the projections of two radial vectors passing through residues i and j, respectively, in the radial section of the nanotube, and the corresponding distance d separating i and j projected onto the longitudinal axis of the SWNT.

nanoseconds later, this end of the chain comes back by virtue of van der Waals attraction, thereby allowing the perfect helical structure to be recovered. The pitch over the last 60 ns of the simulation averaged out to 14.6 ± 1.7 nm.

To investigate further the role of the SWNT on the conformation of the CHTS chain, an additional 30 ns MD simulation of the latter was performed in water, in the absence of the SWNT. The torsional angles that characterize the backbone conformation of the polysaccharide chain were examined. Toward this end, a pair of backbone torsional angles describing the glycosidic linkage between two adjacent monomers was defined as φ (C2−C1−O1−C4′) and ψ (C1−O1−C4′−C3′); see Scheme 1. The values of φ and ψ in the crystal are 145.9° and 94.1°, respectively. An overview of the (φ,ψ)-distribution after equilibration can be found in Figure 2a and b. The distribution for the free CHTS primarily peaks in the region defined by $150° \leq \varphi \leq 200°$ and $100° \leq \psi \leq 140°$. In the presence of the SWNT, the distribution shifts toward smaller φ and ψ angles and almost breaks up into two regions. This distinct modification of backbone torsional angles can be ascribed to the helical, wrapping conformation of the CHTS chain induced by the SWNT. It can be contended from the latter that SWNTs can be used as templates to modulate the spatial structure of free CHTS.

In addition, the average ψ torsional angle was monitored over the entire trajectory. As illustrated in Figure 2c, this angle increases gradually and reaches a maximum value, which corresponds to the minimum of the helical pitch. In contrast, the time evolution of dihedral angle φ did not reveal any obvious trend related to the wrapping process (Figure S1).

3.2. Wrapping Free Energy as a Function of the Pitch. The pitch of the CHTS chain wrapping the nanotube is of paramount

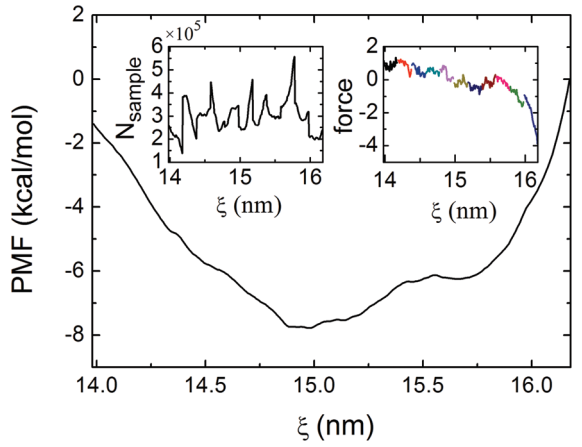

Figure 3. Free-energy profile describing the conformational transition of the CHTS chain around the SWNT, from a straight conformation to a tight helical one. The reference state characterized arbitrarily by a zero free energy, that is, at ξ = 16.2 nm, corresponds to a fully extended CHTS chain adsorbed on the tubular surface. Insets: Number of samples accrued per bin and average force (kcal/mol/Å^2).

importance for condensation of DNA. A suitable pitch could effectively disperse the positive charges and enable CHTS to interact adequately with the grooves of DNA. As mentioned previously, however, the pitch fluctuates within some range due to the diffusion of the termini, as seen from MD trajectory. The free-energy landscape that relates the wrapping process to the pitch was explored by stretching the two ends of the CHTS chain.

As highlighted in Figure 3, the free-energy curve possesses two shallow valleys. As the distance, ξ, separating the two ends of the CHTS chain increases gradually, the free energy drops quickly until it reaches a minimum of about −7.8 kcal/mol with respect to the straight chain, which corresponds to a perfect helical structure with a 13.5 ± 0.9 nm pitch. This minimum prefaces a barrier beyond which a second minimum can be found with 1.5 kcal/mol higher and a pitch of 21.7 ± 1.9 nm. In the latter conformation, the helix loosens up and consists of only one single turn. The free energy subsequently increases in a steady fashion until a straight conformation of the chain is attained. The final state of the transformation is essentially identical to the initial conformation used in the equilibrium MD simulation described previously. The average pitch measured in the MD simulation approaches the one corresponding to the free-energy minimum.

Furthermore, the average pitch and torsional angle ψ were monitored in the course of the reversible stretching process; see Figure 4. As expected, the pitch increases nonlinearly with the end-to-end distance of the chain. The marginal change of the pitch, when the order parameter decreases below 14.5 nm, justifies a posteriori the lower bound of 14.0 nm. It is suggested that the pitch would not change appreciably even though the end-to-end distance were to be shrunk. In sharp contrast, the pitch varies dramatically toward the upper bound of the order parameter, that is, where the CHTS chain approaches its fully extended conformation.

The backbone torsional angle ψ constitutes evidently the key parameter that determines the size of the pitch. Figure 4 reveals a steady decrease of its average as the pitch increases. The van der Waals attraction exerted by the nanotube modulates the intrinsic torsional preference of the free CHTS backbone through β-1, 4 linking and accordingly alters the corresponding equilibrium

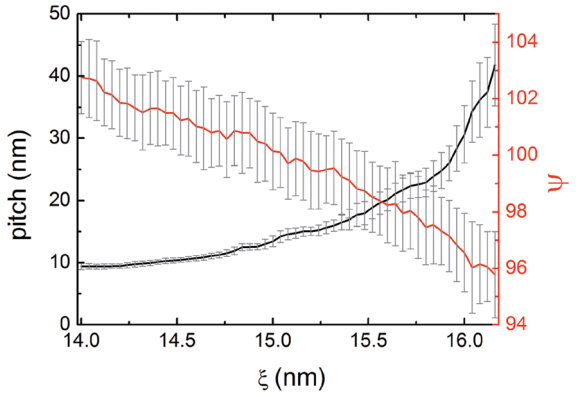

Figure 4. The average pitch (black) and average torsional angle ψ (red) as a function of the order parameter, ξ.

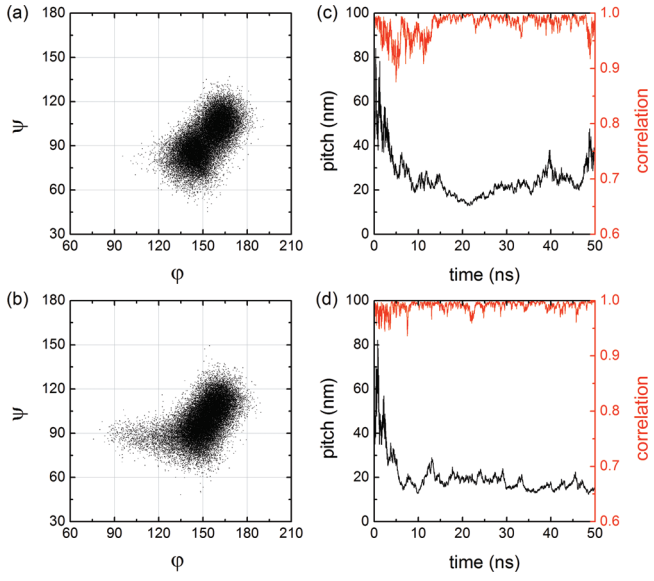

Figure 5. (a) Distribution of the (φ,ψ) backbone torsional angles for (a) CHIT and (b) CHTS (nonionic). Time evolution of the pitch (black) and angle−distance correlation (red) for (c) CHIT and (d) CHTS (nonionic).

distribution. The free-energy favored conformations are envisioned to arise from a competitive balance between van der Waals attraction and torsional preferences.

3.3. Role of pH and Deacetylation. Chitosan is produced via deacetylation of CHIT. Yet, reaching a degree of deacetylation equal to 100% is extremely challenging. This polysaccharide is generally referred to as chitosan if deacetylation exceeds 50%, a level at which the macromolecule becomes soluble in aqueous acidic media. Protonation of the amine moieties in the glucosamine units induces the solubilization. Besides, such amine groups are important sites for metal−ion chelation and electrostatic attraction of anions to form stable complexes. Experiment[15] and theory[38] have demonstrated that both the degree of deacetylation and the pH have a pronounced effect on the solubility, the structural properties, and the charge distribution of chitosan. In view of the latter, two extreme cases have been considered to investigate by MD simulation the role played by the pH and the level of deacetylation on the structure of CHTS−SWNT complex: on the one hand, CHIT, viz. 0% deacetylation level, while on the other hand, CHTS utilized previously in an unprotonated form to assess pH effects.

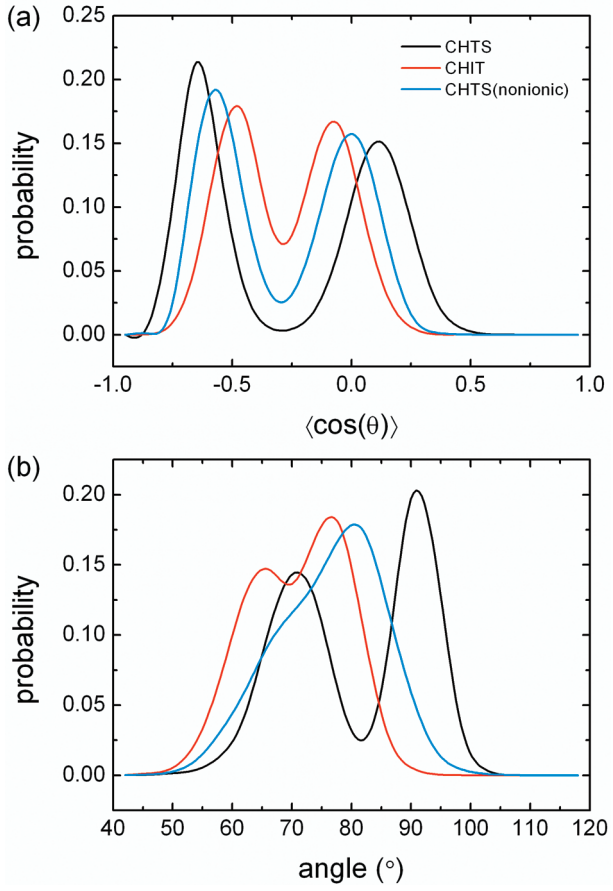

Figure 6. (a) Distribution of the orientational order parameter $\langle\cos(\theta)\rangle$ of bond C2−N2. θ is the angle between the bond vector from C2 to N2 and the *Z*-direction of Cartesian space, that is, the longitudinal axis of the SWNT. (b) Distribution of the orientation angle of the pyranose ring, which is defined as the angle between the normal to the plane of the ring plane formed by atoms C1, C2, C4, and C5, and the longitudinal axis of the SWNT.

The distribution of the backbone torsional angles and the fluctuation of the pitch were calculated for comparison purposes, as depicted in Figure 5. A right-handed helical structure was observed in the two simulations of the polysaccharide chain, albeit their pitch and helicity appear to be at variance. Among all three cases, helicity imperfection was the most pronounced for CHIT. Figure 5c reveals that CHIT is unable to maintain a steady helical conformation over long times, the pitch fluctuating significantly in the course of the simulation. In sharp contrast, both the pitch and the helicity of the nonionic CHTS chain were preserved (see Figure 5d), akin to the homologous ionic chain (Figure 2d). Protonation of amine groups has, therefore, almost no effect on the helical structure of wrapped CHTS. It can be further contended that electrostatic repulsion does not constitute the predominant factor that prevents the pitch from shrinking. This result is different from the work of Klein[12] and our previous study,[36] where electrostatic interactions play an important role in the formation of helical wrapping structure.

The difference in both pitch and helicity is also reflected in the distributions of the backbone torsional angles. The distribution for CHIT is located in the region defined by $120° \leq \varphi \leq 180°$ and $60° \leq \psi \leq 130°$. By comparison, much of the distribution is preserved in nonionic conditions, barring the slight offset toward lower values of φ when ψ ranges from 80° to 100°.

The distinctive structural characteristics of the three examples examined herein concern primarily the functional groups linking the C2 position of the pyranose ring. The orientational order parameter of bond C2−N2, viz. $\langle\cos(\theta)\rangle$, was, hence, computed to describe the local bond orientation after wrapping. The probability distributions gathered in Figure 6a indicate that the C2−N2 bond can adopt two preferred orientations under all three conditions. The bond orientation for the nonionic polysaccharide chain is found between 90° and 125°. As a comparison, the distribution for the ionic CHTS and CHIT is shifted inward and outward, respectively. For CHTS, an orientation at 130° is preferred. Under the influence of pH and the degree of deacetylation, the distance separating the two preferred orientations decreases, and the probability distributions of these two orientations tend to be similar.

In addition, the orientation of the pyranose ring was investigated. As shown in Figure 6b, the probability distribution for CHTS splits into two distinct peaks, the maximum of which arises at 70° and 90°, respectively. It follows from the latter that most rings prefer to lie parallel to the surface of the SWNT. In the other cases, in contrast, the distributions shift toward the left-hand side, suggesting that the ring preferentially tilts toward the tubular surface.

4. CONCLUSIONS

Gene delivery is the optimal route for gene therapy. Effective condensation of DNA into nanoparticles constitutes a crucial prerequisite for the transport of the therapeutic gene toward its target. Recent experiments[16,17] have shown that CNTs coated with CHTS or its derivatives can significantly enhance DNA condensation.

In the present work, large-scale atomistic MD simulations have been conducted to explore the self-assembly and the structural characteristics of CHTS−SWNT complexes in explicit aqueous environment. The CHTS chain is able to wrap spontaneously the tubular surface by virtue of van der Waals attraction, resulting in a perfect helical conformation. The helix loosens up and cannot be preserved when the degree of deacetylation approaches 0%. The stability of the helix remains, however, unaffected by the pH-dependent charge density of the CHTS chain. The lower pH of the solution could effectively increase the charge density due to the protonation of the amino groups. The high cationic density as well as the dispersion of CHTS by the nanotube through an orderly wrapping allow the complex to interact adequately with the negatively charged DNA, condensing it in a sequential fashion.

The free-energy landscape characterizing the size of the helical pitch was obtained with the aid of the well-suited ABF method.[20−23] The present results reveal that the wrapping process of the polymeric chain around the SWNT features two energetically favored helical conformations. This method can be employed to estimate the pitch of the most stable helical structure, as well as to predict its stability with respect to an extended conformation. A suitable pitch is pivotal for the $-NH^{3+}$ cations of CHTS or for the functional groups of modified CHTS to interact tightly with the grooves of DNA, thereby inducing effective DNA condensation. The free-energy calculations performed in this work may, therefore, provide a possible route for designing functionalized polymers wrapped on CNTs as promising DNA concentrators.

Other important issues, including the curvature of the CNTs, the degree of polymerization of the chain, and the relative concentration, are likely to influence self-assembly. They, however, fall beyond the scope of the present study and ought to be considered

for future computational investigations. The results reported herein shed, nonetheless, meaningful light on the microscopic detail of CHTS−SWNT supramolecular assembly. On the basis of this preliminary exploration, the interactions of this novel assembly and DNA will be investigated in our next work, which would further improve the understanding of DNA condensation toward gene delivery.

■ ASSOCIATED CONTENT

Supporting Information. Detail on the molecular systems investigated and the simulations. Time evolution of the average backbone torsion angle of φ. This material is available free of charge via the Internet at http://pubs.acs.org.

■ AUTHOR INFORMATION

Corresponding Author

*E-mail: wscai@nankai.edu.cn.

Notes

§On leave from Équipe de Dynamique des Assemblages Membranaires, UMR 7565, Nancy Université, BP 239, 54506 Vandoeuvre-lès-Nancy cedex, France.

■ ACKNOWLEDGMENT

This study was supported by the National Natural Science Foundation of China (nos. 20873066 and 20835002).

■ REFERENCES

(1) Ferber, D. *Science* **2001**, *294*, 1638–1642.
(2) Vijayanathan, V.; Thomas, T.; Shirahata, A.; Thomas, T. J. *Biochemistry* **2001**, *40*, 13644–13651.
(3) Matulis, D.; Rouzina, I.; Bloomfield, V. A. *J. Am. Chem. Soc.* **2002**, *124*, 7331–7342.
(4) Choi, J. S.; Joo, D. K.; Kim, C. H.; Kim, K.; Park, J. S. *J. Am. Chem. Soc.* **2000**, *122*, 474–480.
(5) Cai, D.; Mataraza, J. M.; Qin, Z. H.; Huang, Z. P.; Huang, J. Y.; Chiles, T. C.; Carnahan, D.; Kempa, K.; Ren, Z. F. *Nat. Methods* **2005**, *2*, 449–454.
(6) Tasis, D.; Tagmatarchis, N.; Bianco, A.; Prato, M. *Chem. Rev.* **2006**, *106*, 1105–1136.
(7) Kam, N. W. S.; Jessop, T. C.; Wender, P. A.; Dai, H. J. *J. Am. Chem. Soc.* **2004**, *126*, 6850–6851.
(8) Kam, N. W. S.; Liu, Z.; Dai, H. J. *J. Am. Chem. Soc.* **2005**, *127*, 12492–12493.
(9) Kam, N. W. S.; Dai, H. J. *J. Am. Chem. Soc.* **2005**, *127*, 6021–6026.
(10) Pantarotto, D.; Briand, J. P.; Prato, M.; Bianco, A. *Chem. Commun.* **2004**, 16–17.
(11) Singh, R.; Pantarotto, D.; McCarthy, D.; Chaloin, O.; Hoebeke, J.; Partidos, C. D.; Briand, J. P.; Prato, M.; Bianco, A.; Kostarelos, K. *J. Am. Chem. Soc.* **2005**, *127*, 4388–4396.
(12) Johnson, R. R.; Johnson, A. T. C.; Klein, M. L. *Nano Lett.* **2008**, *8*, 69–75.
(13) Johnson, R. R.; Kohlmeyer, A.; Johnson, A. T. C.; Klein, M. L. *Nano Lett.* **2009**, *9*, 537–541.
(14) Johnson, R. R.; Johnson, A. T. C.; Klein, M. L. *Small* **2010**, *6*, 31–34.
(15) Rinaudo, M. *Prog. Polym. Sci.* **2006**, *31*, 603–632.
(16) Kumar, A.; Jena, P. K.; Behera, S.; Lockey, R. F.; Mohapatra, S. *J. Biomed. Nanotechnol.* **2005**, *1*, 392–396.
(17) Liu, Y.; Yu, Z. L.; Zhang, Y. M.; Guo, D. S.; Liu, Y. P. *J. Am. Chem. Soc.* **2008**, *130*, 10431–10439.
(18) Zhang, M. G.; Smith, A.; Gorski, W. *Anal. Chem.* **2004**, *76*, 5045–5050.
(19) Zhang, X. K.; Meng, L. J.; Lu, Q. H. *ACS Nano* **2009**, *3*, 3200–3206.
(20) Darve, E.; Pohorille, A. *J. Chem. Phys.* **2001**, *115*, 9169–9183.
(21) Rodriguez-Gomez, D.; Darve, E.; Pohorille, A. *J. Chem. Phys.* **2004**, *120*, 3563–3578.
(22) Hénin, J.; Chipot, C. *J. Chem. Phys.* **2004**, *121*, 2904–2914.
(23) Hénin, J.; Fiorin, G.; Chipot, C.; Klein, M. L. *J. Chem. Theory Comput.* **2009**, *6*, 35–47.
(24) Sikorski, P.; Hori, R.; Wada, M. *Biomacromolecules* **2009**, *10*, 1100–1105.
(25) Okuyama, K.; Noguchi, K.; Miyazawa, T.; Yui, T.; Ogawa, K. *Macromolecules* **1997**, *30*, 5849–5855.
(26) MacKerell, A. D.; Bashford, D.; Bellott, M.; Dunbrack, R. L.; Evanseck, J. D.; Field, M. J.; Fischer, S.; Gao, J.; Guo, H.; Ha, S.; Joseph-McCarthy, D.; Kuchnir, L.; Kuczera, K.; Lau, F. T. K.; Mattos, C.; Michnick, S.; Ngo, T.; Nguyen, D. T.; Prodhom, B.; Reiher, W. E.; Roux, B.; Schlenkrich, M.; Smith, J. C.; Stote, R.; Straub, J.; Watanabe, M.; Wiorkiewicz-Kuczera, J.; Yin, D.; Karplus, M. *J. Phys. Chem. B* **1998**, *102*, 3586–3616.
(27) Phillips, J. C.; Braun, R.; Wang, W.; Gumbart, J.; Tajkhorshid, E.; Villa, E.; Chipot, C.; Skeel, R. D.; Kale, L.; Schulten, K. *J. Comput. Chem.* **2005**, *26*, 1781–1802.
(28) Kuttel, M.; Brady, J. W.; Naidoo, K. J. *J. Comput. Chem.* **2002**, *23*, 1236–1243.
(29) Jorgensen, W. L.; Chandrasekhar, J.; Madura, J. D.; Impey, R. W.; Klein, M. L. *J. Chem. Phys.* **1983**, *79*, 926–935.
(30) Ryckaert, J. P.; Ciccotti, G.; Berendsen, H. J. C. *J. Comput. Phys.* **1977**, *23*, 327–341.
(31) Andersen, H. C. *J. Comput. Phys.* **1983**, *52*, 24–34.
(32) Darden, T.; York, D.; Pedersen, L. *J. Chem. Phys.* **1993**, *98*, 10089–10092.
(33) Feller, S. E.; Zhang, Y.; Pastor, R. W.; Brooks, B. R. *J. Chem. Phys.* **1995**, *103*, 4613–4621.
(34) Humphrey, W.; Dalke, A.; Schulten, K. *J. Mol. Graphics* **1996**, *14*, 33–38.
(35) Liu, Y.; Liang, P.; Zhang, H.; Guo, D. *Small* **2006**, *2*, 874–878.
(36) Liu, Y. Z.; Chipot, C.; Shao, X. G.; Cai, W. S. *J. Phys. Chem. B* **2010**, *114*, 5783–5789.
(37) Kang, Y. K.; Lee, O. S.; Deria, P.; Kim, S. H.; Park, T. H.; Bonnell, D. A.; Saven, J. G.; Therien, M. J. *Nano Lett.* **2009**, *9*, 1414–1418.
(38) Franca, E. F.; Lins, R. D.; Freitas, L. C. G.; Straatsma, T. P. *J. Chem. Theory Comput.* **2008**, *4*, 2141–2149.